

$SU(2)$ principal chiral model with tensor renormalization group on a cubic lattice

Shinichiro Akiyama^{1,2,*} Raghav G. Jha^{3,†} and Judah Unmuth-Yockey^{4,‡}

¹Center for Computational Sciences, University of Tsukuba, Tsukuba, Ibaraki 305-8577, Japan

²Graduate School of Science, The University of Tokyo, Bunkyo-ku, Tokyo 113-0033, Japan

³Thomas Jefferson National Accelerator Facility, Newport News, Virginia 23606, USA

⁴Fermi National Accelerator Laboratory, Batavia, Illinois, USA



(Received 1 July 2024; accepted 8 August 2024; published 30 August 2024)

We study the continuous phase transition and thermodynamic observables in the three-dimensional Euclidean $SU(2)$ principal chiral field model with the triad tensor renormalization group and the anisotropic tensor renormalization group methods. Using these methods, we find results that are consistent with previous Monte Carlo estimates and the predicted renormalization group scaling of the magnetization close to criticality. These results bring us one step closer to studying finite-density quantum chromodynamics in four dimensions using tensor network methods.

DOI: [10.1103/PhysRevD.110.034519](https://doi.org/10.1103/PhysRevD.110.034519)

I. INTRODUCTION

In recent decades, significant progress has been made in understanding the nonperturbative physics of quantum chromodynamics (QCD) through lattice gauge theory based on Wilson’s insights. However, a major challenge in the Monte Carlo (MC) simulations arises when attempting to compute real-time dynamics or simulate at finite-baryon density (chemical potential) or in the presence of topological theta term. This obstacle is primarily due to a signal-to-noise issue called the “sign problem,” where relevant gauge-invariant quantities are exponentially suppressed relative to their error margins. This hinders a comprehensive understanding of the QCD phase diagram at finite baryon density and temperature which is crucial for a proper understanding of a wide range of rich phenomena. For a recent comprehensive review, we refer the reader to Refs. [1,2].

Given the limitations of existing sampling-based numerical tools, there is a growing interest in exploring alternative methods ranging from classical tensor networks to quantum computing. Tensor network techniques, particularly when integrated into a blocking algorithm known as the “tensor renormalization group” (TRG) [3], have shown promise in

addressing these limitations. While TRG methods have been successfully applied to several spin systems and lattice gauge theories [4–23], efforts to employ them in studying models in more than two Euclidean dimensions have still been difficult. This difficulty was addressed by TRG algorithms which scale better in a larger number of dimensions [24–27] compared to the higher-order TRG (HOTRG), a variant of the TRG method, which scales like $O(D^{4d-1})$ in d -dimensional Euclidean systems with bond dimension D [28].

Two prominent approaches are the triad TRG (tTRG) [26], and the anisotropic TRG (ATRG) [24], which are the main focus of this work. Both these algorithms have improved scaling in computational time and memory relative to the HOTRG algorithm, with the computational time in the tTRG scaling like $O(D^{d+3})$, and the ATRG scaling like $O(D^{2d+1})$. These two TRG algorithms have been applied for various higher-dimensional lattice theories [18,19,21,29–34]. However, even with the improved time complexity, the two methods make additional approximations in different ways leading to them potentially discarding different physics during coarse-graining. Because of these differences, it is important to quantify their respective efficacies to understand which approximations are superior, if at all.

A further difficulty is the computational cost associated with tensor formulations of actions possessing non-Abelian symmetries [35–37]. These non-Abelian symmetries prompt the existence of additional quantum numbers, giving rise to more complicated constraints between degrees of freedom. The transition from Abelian symmetries, where simple conservation-law constraints appear, to non-Abelian symmetries where milder constraints

*Contact author: akiyama@ccs.tsukuba.ac.jp

†Contact author: raghav.govind.jha@gmail.com

‡Contact author: jfunmuthyockey@gmail.com

manifest, e.g., triangle inequalities, drastically increases the memory cost of tensor networks. Because of this, the algorithmic improvements provided by the tTRG and the ATRG are encouraging, but it is still unclear how these algorithms handle these constraints under blocking.

To understand the potential of these algorithms as a means to eventually probe QCD, it is often useful to consider simpler models with similar properties. Notably, it has been suggested that the chiral phase transition in the two massless flavors approximation of QCD shares critical exponents with the three-dimensional $SU(2)$ principal chiral model ($O(4)$ nonlinear sigma model) [38–42]. Leveraging this connection, investigations have been conducted using MC and other numerical approaches to shed light on this model [43–49].

In this study, we focus on exploring the three-dimensional $SU(2)$ principal chiral model using tensor network methods. We construct the tensor network representation for the path integral based on the character expansion, which allows us to preserve the original $SU(2)$ symmetry even after the finite truncation of the irreducible representations. Since the symmetry is preserved, it is naturally expected that we can obtain the correct scaling behavior of the $O(4)$ model. We note that this kind of truncation effect has been recently investigated in the two-dimensional $O(2)$ model with tensor network methods [50] and our work is the first tensorial attempt in three dimensions extending the preliminary work by authors in Ref. [51]. By employing the ATRG and tTRG algorithms, the goal is to compute canonical quantities such as internal energy, magnetization, and the critical coupling associated with the continuous phase transition. We also comment on the critical exponents and the fixed-point behavior of the algorithms used in this paper.

II. THE MODEL

The $SU(2)$ principal chiral model in three dimensions has a continuum action given by

$$S = \frac{J}{4} \int d^3x \text{Tr} \left[\sum_{\nu=1}^3 \partial_{\nu} U(x)^{\dagger} \partial_{\nu} U(x) \right], \quad (2.1)$$

where J is the coupling constant and $U(x)$ are elements of $SU(2)$. The action in (2.1) is invariant under an $SU(2)_L \otimes SU(2)_R$ global symmetry which acts on U and U^{\dagger} as $U(x) \rightarrow G_L U(x) G_R^{\dagger}$ and $U^{\dagger}(x) \rightarrow G_R U^{\dagger}(x) G_L^{\dagger}$ where G is an element of the $SU(2)$. This model is equivalent to the $O(4)$ nonlinear sigma model because of the well-known homomorphism i.e., $SU(2) \otimes SU(2) \equiv SO(4)$ and was first considered by Polyakov as a toy model to understand the chiral symmetry breaking in QCD [52]. The Euclidean lattice action is:

$$S = -\frac{J}{2} \sum_{n,\nu} \text{Tr}[U(n)U(n+\hat{\nu})^{\dagger}], \quad (2.2)$$

where the $SU(2)$ group elements live on the sites, n , of the lattice, and the ν -sum is over the three orthogonal directions of the cubic lattice. The path integral on the lattice is given by

$$Z = \int \prod_n dU(n) e^{-S}, \quad (2.3)$$

and the group integration is the typical Haar integral. We assume periodic boundary conditions for all directions.

The average internal energy density can be defined by a derivative of the thermodynamic potential $f(J) \equiv -\log Z(J)$,

$$\langle e \rangle = \frac{1}{V} \frac{\partial}{\partial J} f(J). \quad (2.4)$$

One can explicitly break the global symmetry by including an external field term in the action,

$$S_H = -H \sum_n \text{Tr}[U(n)]. \quad (2.5)$$

The average value of this on-site interaction term can also be defined using a derivative of $f(J, H)$,

$$\langle m \rangle \equiv \frac{1}{V} \left\langle \sum_n \text{Tr}[U(n)] \right\rangle = -\frac{1}{V} \frac{\partial}{\partial H} f(J, H). \quad (2.6)$$

In the following section we will provide tensor network descriptions of the path integral and these expectation values, along with one more useful quantity.

A. Tensor network construction

Tensor network constructions for this model without S_H have been considered before in Refs. [35,36,49]. Here we briefly review the construction using the character expansion method, as well as provide a construction in the case of an external field.

1. Basic construction

Our goal is to represent Eq. (2.3) as a tensor network such that

$$Z = \text{tTr} \left[\prod_n T_n \right], \quad (2.7)$$

where tTr is the tensor trace over all indices, and T_n is a tensor at site n whose indices are suppressed. Using the character expansion [53,54], we have

$$\begin{aligned} & \exp \left[\frac{J}{2} \text{Tr}[U(n)U(n + \hat{v})^\dagger] \right] \\ &= \sum_r F_r(J) \chi_r(U(n)U(n + \hat{v})^\dagger), \end{aligned} \quad (2.8)$$

with the coefficients written in terms of the modified Bessel function of the first kind as:

$$F_r(J) = \frac{2(2r + 1)}{J} I_{2r+1}(J). \quad (2.9)$$

Since the character $\chi_r(U)$ is the trace of the matrix representation of the group element U in the irreducible

representation of r , we have,

$$\begin{aligned} \chi_r(U(n)U(n + \hat{v})^\dagger) &= \sum_{m,k} D_{mk}^{(r)}(U(n)) \\ &\times D_{mk}^{(r)*}(U(n + \hat{v})). \end{aligned} \quad (2.10)$$

This allows each group element to be integrated individually, generating constraints associated with the sites of the lattice involving Clebsch-Gordan coefficients. After completing all the integrals, a local tensor at a site n is given by

$$\begin{aligned} T_{n;xyz'z'y'x'} &= \sqrt{\prod_{p=1}^6 F_{r_p}(J)} \sum_{R=|r_1-r_2|}^{r_1+r_2} \sum_{R''=|R-r_3|}^{R+r_3} \sum_{R''=|r_4-R'|}^{r_4+R'} \sum_{R'=|r_5-r_6|}^{r_5+r_6} \sum_{M,N} \sum_{M''',N'''} \sum_{M'',N''} \sum_{M',N'} \\ &\times C_{r_1 m_1 r_2 m_2}^{RM} C_{r_1 n_1 r_2 n_2}^{RN} C_{R M r_3 m_3}^{R''M'''} C_{R N r_3 n_3}^{R''N'''} C_{r_4 m_4 R' M'}^{R''M''} C_{r_4 n_4 R' N'}^{R''N''} C_{r_5 m_5 r_6 m_6}^{R'M'} C_{r_5 n_5 r_6 n_6}^{R'N'} \\ &\times \frac{1}{2R'''+1} \delta_{R''',R''} \delta_{M''',M''} \delta_{N''',N''}, \end{aligned} \quad (2.11)$$

where $C_{j_1 m_1 j_2 m_2}^{j m}$ is the Clebsch-Gordan coefficient and $x \equiv (r_1 m_1 n_1)$ is the collective index notation used often going forward. This tensor can be understood in terms of a sequence of smaller tensor contractions—whose nonzero elements are given by the Clebsch-Gordan

coefficients—which are illustrated in Fig. 1. The tensor in Eq. (2.11) can be inserted into Eq. (2.7) for an expression of the path integral using a tensor network contraction.

The field regularization is achieved by introducing a cutoff parameter r_{\max} in Eq. (2.8) as

$$\exp \left[\frac{J}{2} \text{Tr}[U(n)U(n + \hat{v})^\dagger] \right] \simeq \sum_{r=0}^{r_{\max}} F_r(J) \chi_r(U(n)U(n + \hat{v})^\dagger), \quad (2.12)$$

which preserves the global symmetry and does not affect the integration. Using identical methods, we can express the expectation value given in Eq. (2.4) as a ratio of two tensor network contractions.

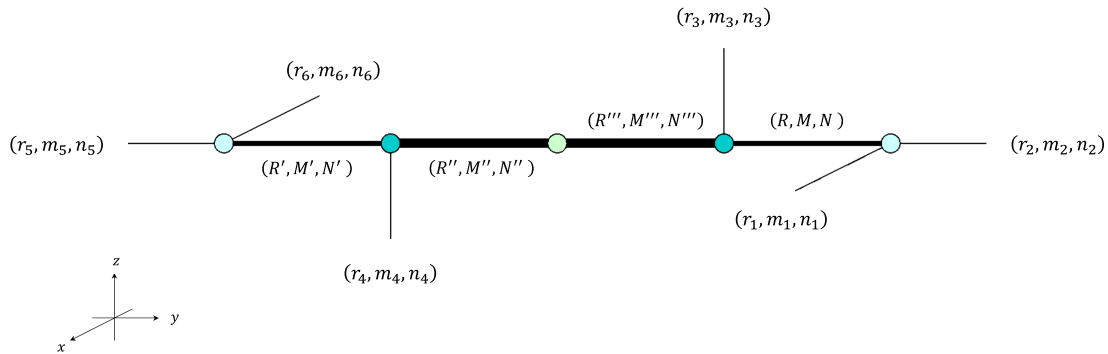


FIG. 1. Tensor network diagram of Eq. (2.11). Each three-leg tensor denotes the Clebsch-Gordan coefficients and the two-leg tensor at the center represents Kronecker delta function. Equation (2.20) is also denoted by the same diagram but with Eq. (2.21) as the matrix at the center. Due to the fusion rule, internal lines have larger bond dimensions than external ones, as shown by their thickness.

2. Impurity tensor for average action

Using the expressions in Eqs. (2.4) and (2.8), the derivative of $f(J)$ affects the character expansion in the following way:

$$\begin{aligned} \frac{\partial}{\partial J} \exp \left[\frac{J}{2} \text{Tr}[U(n)U(n+\hat{\nu})^\dagger] \right] &\simeq \sum_{r=0}^{r_{\max}} \frac{\partial F_r(J)}{\partial J} \chi_r(U(n)U(n+\hat{\nu})^\dagger) \\ &= \sum_{r=0}^{r_{\max}} \tilde{F}_r(J) \chi_r(U(n)U(n+\hat{\nu})^\dagger), \end{aligned} \quad (2.13)$$

with

$$\tilde{F}_r(J) = \frac{2(2r+1)}{J^2} [2rI_{2r+1}(J) + JI_{2r+2}(J)]. \quad (2.14)$$

This minor modification gives an expression for $\langle e \rangle$ in terms of a tensor network that includes two adjacent ‘‘impurities,’’

$$\langle e \rangle = -\frac{3}{Z} \text{tTr} \left[R_{n+\hat{\nu}} S_n \prod_{n' \neq n, n+\hat{\nu}} T_{n'} \right], \quad (2.15)$$

and is the ratio of two scalars, tensor network contractions. This is possible because of the translation invariance of our lattice. The impurities are given by

$$R_{n+\hat{\nu};xyzzy'x'} = \sqrt{\frac{\tilde{F}_{r'}(J)}{F_{r'}(J)}} T_{n+\hat{\nu};xyzzy'x'}, \quad (2.16)$$

and

$$S_{n;xyzzy'x'} = \sqrt{\frac{\tilde{F}_{r'}(J)}{F_{r'}(J)}} T_{n;xyzzy'x'}. \quad (2.17)$$

Note that the ν -directional coarse-graining should be carried out first. We will now discuss the construction of a tensor network when the model includes an external field term in the action.

3. Pure and Impure tensors for magnetization

Consider the action now with an external field term,

$$S = -\frac{J}{2} \sum_{n,\nu} \text{Tr}[U(n)U(n+\hat{\nu})^\dagger] - H \sum_n \text{Tr}[U(n)]. \quad (2.18)$$

In this case, we need to modify the pure tensor, because we have to deal with the finite magnetic field, H , which gives us a new exponential factor. This factor can be expanded as before, giving

$$e^{H \text{Tr}[U(n)]} = \sum_{r_H} F_{r_H}(2H) \chi_{r_H}(U(n)) = \sum_{r_H} F_{r_H}(2H) \sum_{m_H=-r_H}^{r_H} D_{m_H m_H}^{(r_H)}(U(n)), \quad (2.19)$$

where F_{r_H} is defined as in Eq. (2.9). We can use the character expansion to isolate the individual group elements and perform the Haar integration over each one. The integrals from before, in the absence of an external field, are modified but straightforward. The resulting local tensor at site n is given by,

$$\begin{aligned} T_{n;xyzzy'x'} &= \sqrt{\prod_{p=1}^6 F_{r_p}(J)} \sum_{R=|r_1-r_2|}^{r_1+r_2} \sum_{R''=|R-r_3|}^{R+r_3} \sum_{R'=|r_4-R'|}^{r_4+R'} \sum_{R''=|r_5-r_6|}^{r_5+r_6} \sum_{M,N} \sum_{M''} \sum_{M'''} \sum_{M'''} \sum_{M'''} \\ &\times C_{r_1 m_1 r_2 m_2}^{RM} C_{r_1 n_1 r_2 n_2}^{RN} C_{R M r_3 m_3}^{R'' M''} C_{R N r_3 n_3}^{R'' N''} C_{r_4 m_4 R' M'}^{R'' M''} C_{r_4 n_4 R' N'}^{R'' N''} C_{r_5 m_5 r_6 m_6}^{R' M'} C_{r_5 n_5 r_6 n_6}^{R' N'} \\ &\times \frac{1}{2R''+1} \sum_{r_H} F_{r_H}(2H) \sum_{m_H=-r_H}^{r_H} C_{R'' M'' r_H m_H}^{R'' M''} C_{R'' N'' r_H m_H}^{R'' N''} \\ &= \sqrt{\prod_{p=1}^6 F_{r_p}(J)} \sum_{R=|r_1-r_2|}^{r_1+r_2} \sum_{R''=|R-r_3|}^{R+r_3} \sum_{R'=|r_4-R'|}^{r_4+R'} \sum_{R''=|r_5-r_6|}^{r_5+r_6} \sum_{M,N} \sum_{M''} \sum_{M'''} \sum_{M'''} \sum_{M'''} \\ &\times C_{r_1 m_1 r_2 m_2}^{RM} C_{r_1 n_1 r_2 n_2}^{RN} C_{R M r_3 m_3}^{R'' M''} C_{R N r_3 n_3}^{R'' N''} C_{r_4 m_4 R' M'}^{R'' M''} C_{r_4 n_4 R' N'}^{R'' N''} C_{r_5 m_5 r_6 m_6}^{R' M'} C_{r_5 n_5 r_6 n_6}^{R' N'} \\ &\times \frac{1}{2R''+1} \sum_{r_H=|R''-R'''}^{R''+R'''} F_{r_H}(2H) C_{R'' M'' r_H(M''-M''')}^{R'' M''} C_{R'' N'' r_H(M''-M''')}^{R'' N''}. \end{aligned} \quad (2.20)$$

Note with an external field there is an intermediate tensor of the form

$$H_{R''R'''}(H) = \frac{1}{2R''+1} \sum_{r_H=|R''-R'''}^{R''+R'''} F_{r_H}(2H) C_{R''M''}^{R''M''} C_{R''N''}^{R''N''} \quad (2.21)$$

which replaces the Kronecker deltas found in Eq. (2.11).

Now, with Eq. (2.14), we can write down the necessary impure tensor for the calculation of the magnetization density in Eq. (2.6),

$$\begin{aligned} Q_{n;xyz'z'y'x'} &= \sqrt{\prod_{p=1}^6 F_{r_p}(J)} \sum_{R=|r_1-r_2|}^{r_1+r_2} \sum_{R''=|R-R_3|}^{R+R_3} \sum_{R'''=|r_4-R'|}^{r_4+R'} \sum_{R''''=|r_5-r_6|}^{r_5+r_6} \sum_{M,N} \sum_{M''} \sum_{M'''} \sum_{M''''} \\ &\times C_{r_1m_1r_2m_2}^{RM} C_{r_1n_1r_2n_2}^{RN} C_{RMr_3m_3}^{R''M''} C_{RNr_3n_3}^{R''N''} C_{r_4m_4R'M'}^{R''M''} C_{r_4n_4R'N'}^{R''N''} C_{r_5m_5r_6m_6}^{R''M''} C_{r_5n_5r_6n_6}^{R''N''} \\ &\times \frac{1}{2R''+1} \sum_{r_H=|R''-R'''}^{R''+R'''} \tilde{F}_{r_H}(2H) C_{R''M''}^{R''M''} C_{R''N''}^{R''N''}. \end{aligned} \quad (2.22)$$

4. Fixed-point tensor analysis

To understand the behavior of the $O(4)$ fixed-point structure in this model and to check the reliability of our coarse-graining procedure, we use the observable introduced in Ref. [55], X . This quantity has the property that when computed using fixed-point tensors T_{ijklmn} —which are invariant under scaling symmetry: $T \rightarrow \Gamma T$ —it is unchanged. In this subsection, we use X to determine the location of J_c i.e., the critical coupling, and to potentially point out the relevant symmetry breaking responsible for the phase transition. This is possible because the fixed-point structure of the tensor after a large number of iterations can be used to identify the ground state degeneracy of the model. In three dimensions, X is defined as:

$$X \equiv \frac{(T_{abcba})^2}{T_{abccb}T_{defea}}, \quad (2.23)$$

with the tensor indices arranged as $T_{xyz'z'y'x'}$ and summation over repeated indices implied. This quantity has the property that when the tensor is a direct sum of n dimension-one tensors, $X = n$, and when it is a simple dimension-one tensor, $X = 1$ (in the disordered phase at high temperatures or small J). We can use this property to identify when the model undergoes a change in its ground state degeneracy corresponding to a phase transition.

B. Definition of initial tensors for tensor renormalization groups

The tensor network contraction formally given in Eq. (2.7) cannot be carried out exactly, except in the most simple of cases. Instead, we use the tTRG and ATRG methods to approximate it. To use these methods, the

primary tensor, T , must be decomposed into an appropriate form for each specific algorithm.

The philosophy of the tTRG is to rewrite the initial tensor into a contraction of four smaller tensors (in three dimensions). For a generic six-indexed tensor in three dimensions, this takes the form,

$$T_{xyz'z'y'x'} = \sum_{a,b,c} A_{xya} B_{azb} C_{bz'c} D_{cy'x'}. \quad (2.24)$$

The principal chiral model naturally takes the form of a triad decomposition. The right-hand side of Eq. (2.24) is in the same form as Eq. (2.11), with an identification of $x = (r_1m_1n_1)$, $x' = (r_6m_6n_6)$ etc. which gives for the triad tensors,

$$A_{xya} = \sqrt{F_{r_1}(J)F_{r_2}(J)} C_{r_1m_1r_2m_2}^{RM} C_{r_1n_1r_2n_2}^{RN} \quad (2.25)$$

$$B_{azb} = \frac{1}{\sqrt{d_{R''}}} \sqrt{F_{r_3}(J)} C_{RMr_3m_3}^{R''M''} C_{RNr_3n_3}^{R''N''} \quad (2.26)$$

$$C_{bz'c} = \frac{1}{\sqrt{d_{R''}}} \sqrt{F_{r_4}(J)} C_{r_4m_4R'M'}^{R''M''} C_{r_4n_4R'N'}^{R''N''} \quad (2.27)$$

$$D_{cy'x'} = \sqrt{F_{r_5}(J)F_{r_6}(J)} C_{r_5m_5r_6m_6}^{R''M''} C_{r_5n_5r_6n_6}^{R''N''}, \quad (2.28)$$

where the index structure makes it clear when we are referring to the Clebsch-Gordan coefficients, and when we are referring to the C tensor. This triad formulation is shown in Fig. 2, with the A , B , C , and D tensors appearing from right to left.

The impure tensors from Eqs. (2.16) and (2.17) can be immediately used in the triad formulation as well. They modify the, say, B and C tensors on two adjacent sites, say,

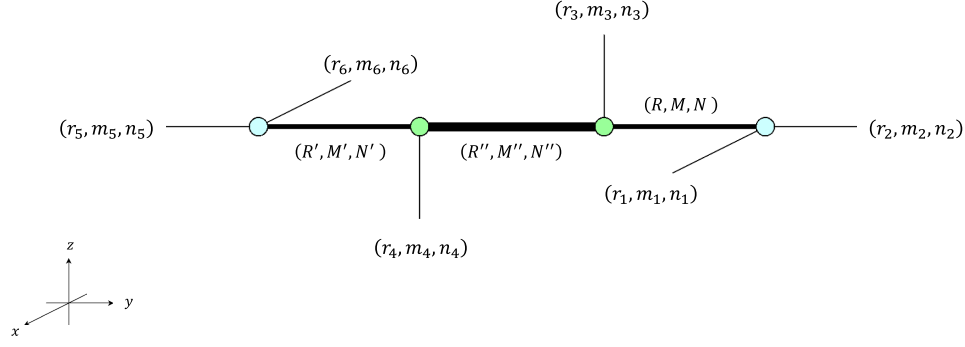
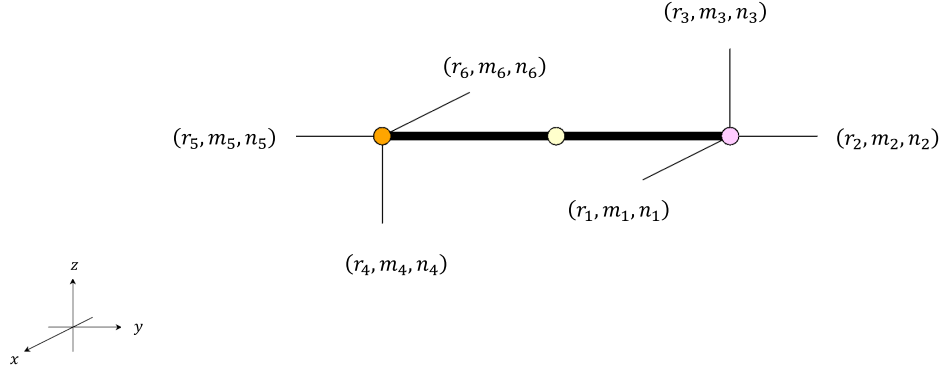


FIG. 2. Initial tensors for the tTRG.

FIG. 3. Initial tensors for the ATRG in Eq. (2.31). Four-leg tensors denote unitary matrices and the two-leg tensor shows the singular value. In the practical computation, the size of the internal line is truncated by the bond dimension D in the ATRG.

n and $n + \hat{z}$, respectively,

$$\begin{aligned} \tilde{B}_{azb}(n) &= \sqrt{\frac{\tilde{F}_{r_3}(J)}{F_{r_3}(J)}} B_{azb}(n) \\ &= \frac{1}{\sqrt{d_{R''}}} \sqrt{\tilde{F}_{r_3}(J)} C_{RM'r_3m_3}^{R''M''} C_{RN'r_3n_3}^{R''N''} \end{aligned} \quad (2.29)$$

$$\begin{aligned} \tilde{C}_{bz'c}(n + \hat{z}) &= \sqrt{\frac{\tilde{F}_{r_4}(J)}{F_{r_4}(J)}} C_{bz'c}(n + \hat{z}) \\ &= \frac{1}{\sqrt{d_{R''}}} \sqrt{\tilde{F}_{r_4}(J)} C_{r_4m_4R'M'}^{R''M''} C_{r_4n_4R'N'}^{R''N''}. \end{aligned} \quad (2.30)$$

For the case of an external field, the H matrix in Eq. (2.21) naturally fits between the B and C tensors.

For the ATRG, we convert T into the canonical form to evaluate Eq. (2.7). This decomposition can be seen in Fig. 3. The canonical form we need is

$$T_{xyzz'y'x'} = \sum_{\gamma} U_{xyz\gamma} \sigma_{\gamma} V_{z'y'x'\gamma}^*, \quad (2.31)$$

which is nothing but the SVD of T . This canonical form can be constructed without using the full six-indexed tensor by using the natural triad structure of the tensor described

above. In the practical computation, we introduce the low-rank approximation in Eq. (2.31) to decimate the smaller singular values up to the bond dimension.

III. RESULTS

With the tensor constructions defined in Sec. II B, we can compute quantities using both the tTRG, and the ATRG, and compare. For this comparison, we consider $\langle e \rangle$, X , and $\langle m \rangle$, and we make the comparison at fixed bond dimension.

The computation of the internal energy can be seen in Fig. 4. This is done using the impure tensor. Here we not only compare the tTRG and the ATRG but also include MC results to provide a cross-check. The relative error,

$$\epsilon_{\text{rel}} = \frac{\langle e \rangle_{\text{TRG}} - \langle e \rangle_{\text{MC}}}{\langle e \rangle_{\text{MC}}}, \quad (3.1)$$

between the tensor calculations and the MC are shown in the inset plot. We find in the “strong-coupling/high-temperature” regime that the tensor results agree well with the MC results. In the “weak-coupling/low-temperature” regime we find poorer accuracy, however, as r_{max} is increased, the tensor results move toward the MC data.

In Fig. 5 we see the comparison between the tTRG and the ATRG in computing X . Previous studies [34,55–58]

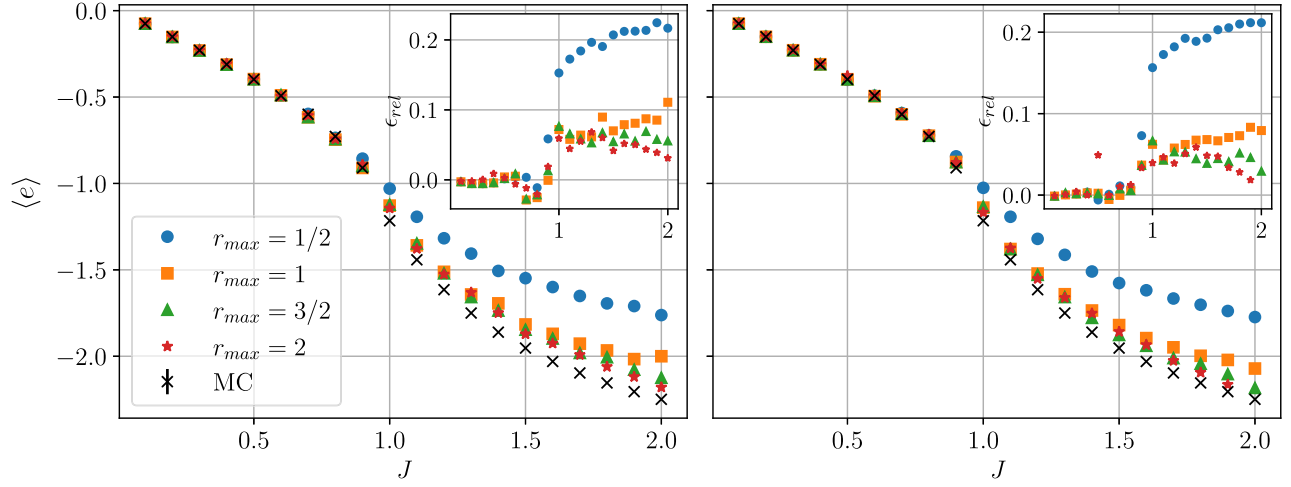


FIG. 4. The average internal energy plotted alongside the MC computation using the tTRG (left) and ATRG (right). In both tensor computations $D = 50$ for the three lowest irreps., and $D = 70$ for $r_{max} = 2$, and $L = 16$.

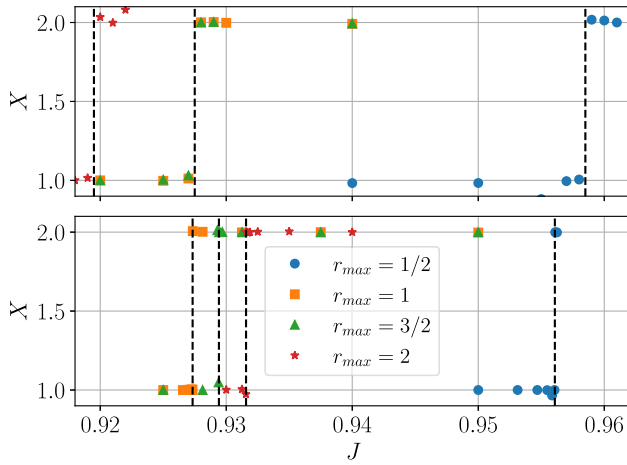


FIG. 5. The X quantity using the tTRG (top) and ATRG (bottom). Both methods used $D = 50$, and $L = 1024$. The vertical dashed lines indicate the estimated values for the various J_c . The correct MC value is $J_c = 0.936(1)$.

focused on computing X in the presence of a discrete global symmetry. Its use as a tool to identify phase transitions for continuous global symmetries is untested. Both tensor methods see a “jump” in X around some J_c , indicating a potential phase transition. We use this jump to identify J_c for various r_{max} values, which we use in later computations of the magnetization. The location of the jumps as a function of r_{max} does not completely agree between the two methods, although they are roughly consistent. However, the tTRG value for J_c with $r_{max} = 1$ and $r_{max} = 3/2$ are the same at this resolution, unlike the ATRG which has two different values for these two r_{max} cutoffs. The tTRG result for $r_{max} = 2$ actually worsens, in contrast to the ATRG.

The values of J_c extracted using this method can be seen plotted against D in Fig. 6. The result obtained using MC

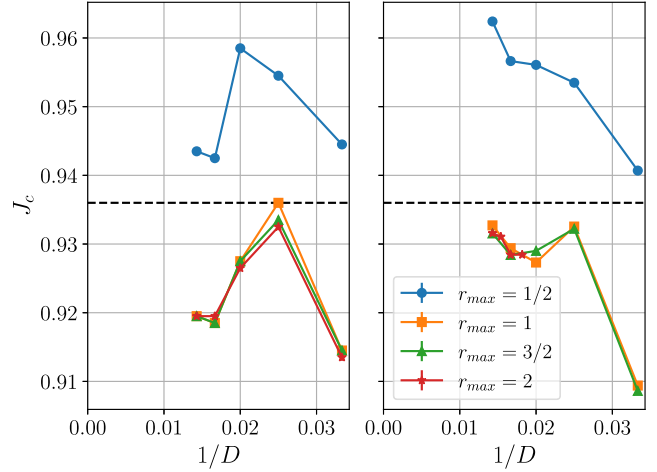


FIG. 6. The critical coupling J_c as determined using X plotted versus $1/D$. The result from MC [43] is shown with a dashed line and an uncertainty that is not visible in the plot.

methods shows $J_c = 0.936(1)$ [43] which is closest to the ATRG result with the highest truncation. It seems that with these results, ATRG does slightly better than tTRG in obtaining a better approximation. It is worth noting that the jump from $X = 1$ to $X = 2$ is reminiscent of a similar jump associated with the Ising universality class. However, as found in MC, as well as in this study, the critical exponents found for the phase transition in this model are not consistent with the Ising type as we will see below.

The final quantity we consider is the magnetization. This quantity is calculated in the presence of an external field using an impure tensor. The results of this calculation can be seen in Fig. 7 for $H = 0.01$. We see somewhat similar results between the tTRG and ATRG, however, at larger J values, the tTRG possesses noise which can be radical for some values of J . We find this effect is both r_{max} and

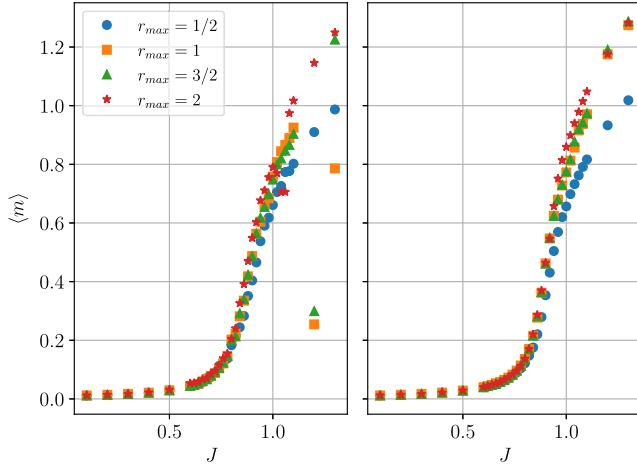


FIG. 7. Magnetization with $H = 0.01$ for tTRG (left) and ATRG (right). We use $D = 50$ for the three smallest irreps. and $D = 70$ for $r_{\max} = 2$. The lattice volume is 1024^3 in all cases.

D dependent. One can also see that the tTRG result is systematically slightly lower than the ATRG result, especially in the large J regime, indicating the tTRG may be missing a fraction of the true critical behavior.

To address this point, we attempt to collapse the magnetization data under the assumption of the existence of a critical point, which was carried out using MC and nonperturbative renormalization group method for this model in Refs. [44,47,59]. We define the following variables,

$$j \equiv \frac{J_c - J}{J_c}, \quad (3.2)$$

and

$$h \equiv \frac{H}{H_0}, \quad (3.3)$$

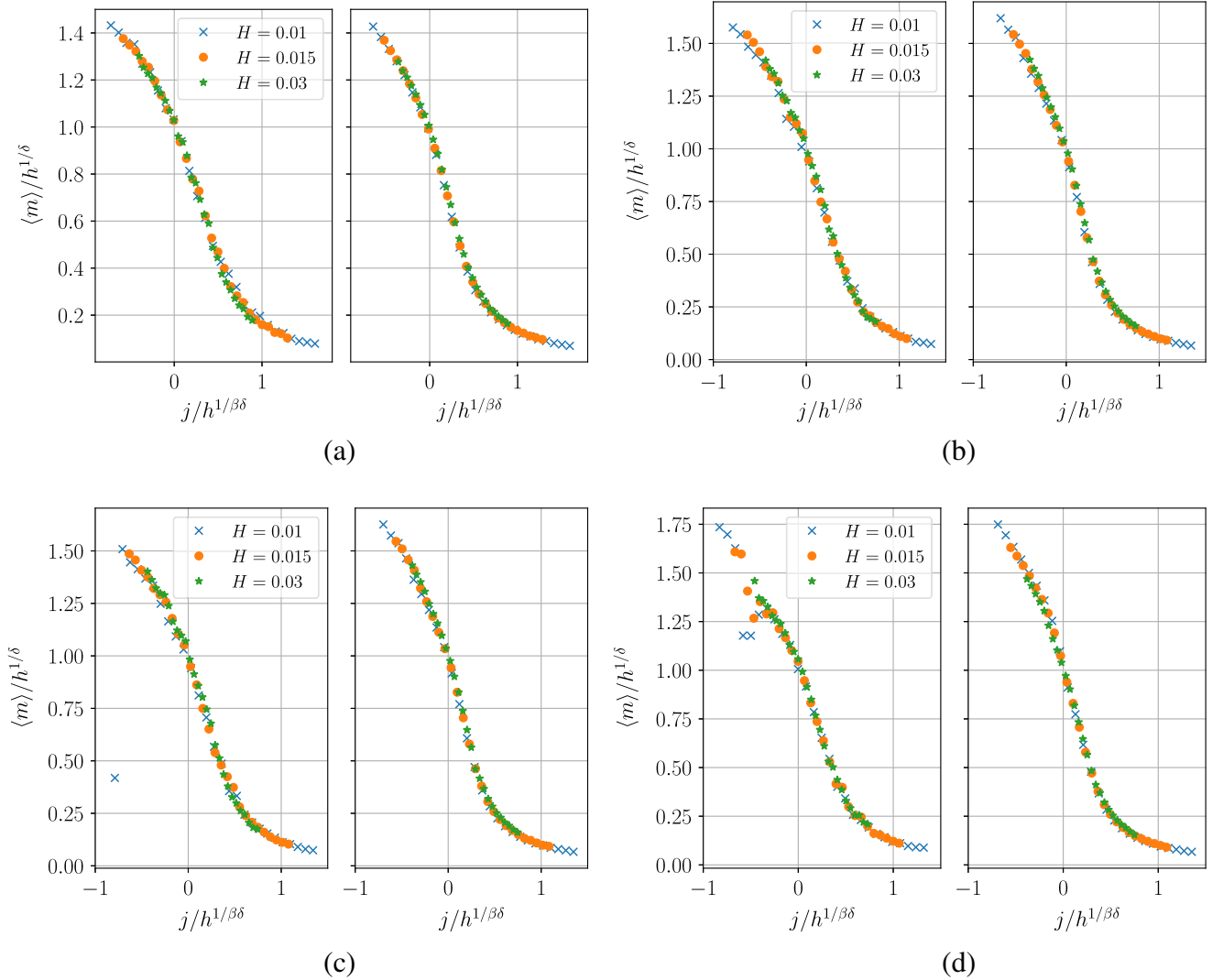


FIG. 8. The magnetization collapse for various truncations. The left panel shows the results using tTRG, and the right panel shows ATRG. (a)–(c) $r_{\max} = 1/2, 1, 3/2$ were calculated with $D = 50$, and (d) $r_{\max} = 2$ was done with $D = 70$. The volume is 1024^3 .

which can be used in the following scaling functional form

$$\frac{\langle m \rangle}{h^{1/\delta}} = f(j/h^{1/\beta\delta}) \quad (3.4)$$

that is valid in the regime of critical behavior. Figure 8 shows the resulting collapsed data for four different truncations. Here H_0 is chosen such that $f(0) = 1$, and β and δ are the usual critical exponents. We use the values from Ref. [43] of $\beta = 0.3836(46)$ and $\delta = 4.851(22)$. The respective values of J_c are determined using the results from the X calculation, for both the tTRG and ATRG collapses. We find the TRG results are consistent with the critical exponents obtained using MC using both methods, indicating that while the tTRG estimate for J_c is worse than the ATRG estimate, the underlying critical behavior captured by it for the magnetic exponents is still consistent with the literature.¹

IV. CONCLUSIONS

We carried out a systematic study of the three-dimensional $SU(2)$ principal chiral model which belongs to the same universality class as the $O(4)$ nonlinear sigma model. This model is useful in understanding chiral symmetry in QCD in a simplified setting. Since our tensor network formulation is based on character expansion, the $SU(2)$ symmetry is explicitly present even with a finite r_{\max} truncation. We used different tensor network algorithms and computed the critical coupling, average action, magnetization, and fixed point observables. In addition, we also compute the RG collapse plots for magnetization which has previously not been attempted using the higher-dimensional TRG approach. Our results show the efficiency of tensor methods even in three Euclidean dimensions to reproduce the expected critical exponents. Our results are also the first direct comparison of observables, calculated using two different methods (ATRG and

¹One can fit α directly from the internal energy using the following expression [28],

$$\langle e \rangle = A + B|J - J_c| + C|J - J_c|^{1-\alpha}, \quad (3.5)$$

where A , B , and C are fit parameters. Using this method, both the tTRG and the ATRG finds α that is consistently negative [51]. However, obtaining a precise value following this way is difficult and we leave this for future work.

tTRG), in a model with a continuous non-Abelian symmetry group in three dimensions.

Generally, we find the ATRG is more accurate and less noisy with respect to the results from the literature; however, the tTRG does correctly capture the critical behavior for the exponents calculated here. Moreover, we note that the tTRG was compared to the ATRG using the same D in all calculations, but that the tTRG possesses superior scaling in computational cost which was not taken advantage of in these calculations. Future studies using the full strength of the tTRG could demonstrate improved accuracy. It would be interesting to improve the algorithms used in this paper such that those computations can be pursued. We leave this improvement and study of gauge theories in three dimensions for future work.

ACKNOWLEDGMENTS

We thank Jacques Bloch for sharing the Monte Carlo data and Katsumasa Nakayama for sharing several data presented in Ref. [26]. S. A. acknowledges the support from the Endowed Project for Quantum Software Research and Education, the University of Tokyo [60], JSPS KAKENHI Grant No. JP23K13096, and the Center of Innovations for Sustainable Quantum AI (JST Grant No. JPMJPF2221). The ATRG calculation for the present work was carried out with ohtaka provided by the Institute for Solid State Physics, the University of Tokyo, and the use of SQUID at the Cybermedia Center, Osaka University (Project ID: hp240012). R. G. J. is supported by the U.S. Department of Energy, Office of Science, National Quantum Information Science Research Centers, Co-design Center for Quantum Advantage (C2QA) under Contract No. DE-SC0012704 and by the U.S. Department of Energy, Office of Science, Office of Nuclear Physics under Contract No. DE-AC05-06OR23177. This manuscript has been co-authored by an employee of Fermi Research Alliance, LLC under Contract No. DE-AC02-07CH11359 with the U.S. Department of Energy, Office of Science, Office of High Energy Physics. This work is supported by the Department of Energy through the Fermilab Theory QuantISED program in the area of “Intersections of QIS and Theoretical Particle Physics”. We thank the Institute for Nuclear Theory at the University of Washington for its kind hospitality and stimulating research environment. This research was supported in part by the INT’s U.S. Department of Energy Grant No. DE-FG02-00ER41132.

- [1] P. de Forcrand, Simulating QCD at finite density, *Proc. Sci. LAT2009* (2009) 010 [arXiv:1005.0539].
- [2] K. Nagata, Finite-density lattice QCD and sign problem: Current status and open problems, *Prog. Part. Nucl. Phys.* **127**, 103991 (2022).
- [3] M. Levin and C. P. Nave, Tensor renormalization group approach to 2D classical lattice models, *Phys. Rev. Lett.* **99**, 120601 (2007).
- [4] Y. Shimizu and Y. Kuramashi, Grassmann tensor renormalization group approach to one-flavor lattice Schwinger model, *Phys. Rev. D* **90**, 014508 (2014).
- [5] Y. Shimizu and Y. Kuramashi, Critical behavior of the lattice Schwinger model with a topological term at $\theta = \pi$ using the Grassmann tensor renormalization group, *Phys. Rev. D* **90**, 074503 (2014).
- [6] B. Dittrich, S. Mizera, and S. Steinhaus, Decorated tensor network renormalization for lattice gauge theories and spin foam models, *New J. Phys.* **18**, 053009 (2016).
- [7] Y. Shimizu and Y. Kuramashi, Berezinskii-Kosterlitz-Thouless transition in lattice Schwinger model with one flavor of Wilson fermion, *Phys. Rev. D* **97**, 034502 (2018).
- [8] J. Unmuth-Yockey, J. Zhang, A. Bazavov, Y. Meurice, and S.-W. Tsai, Universal features of the Abelian Polyakov loop in $1+1$ dimensions, *Phys. Rev. D* **98**, 094511 (2018).
- [9] Y. Kuramashi and Y. Yoshimura, Three-dimensional finite temperature Z_2 gauge theory with tensor network scheme, *J. High Energy Phys.* **08** (2019) 023.
- [10] J. F. Unmuth-Yockey, Gauge-invariant rotor Hamiltonian from dual variables of 3D $U(1)$ gauge theory, *Phys. Rev. D* **99**, 074502 (2019).
- [11] A. Bazavov, S. Catterall, R. G. Jha, and J. Unmuth-Yockey, Tensor renormalization group study of the non-Abelian Higgs model in two dimensions, *Phys. Rev. D* **99**, 114507 (2019).
- [12] Y. Kuramashi and Y. Yoshimura, Tensor renormalization group study of two-dimensional $U(1)$ lattice gauge theory with a θ term, *J. High Energy Phys.* **04** (2020) 089.
- [13] N. Butt, S. Catterall, Y. Meurice, R. Sakai, and J. Unmuth-Yockey, Tensor network formulation of the massless Schwinger model with staggered fermions, *Phys. Rev. D* **101**, 094509 (2020).
- [14] R. G. Jha, Critical analysis of two-dimensional classical XY model, *J. Stat. Mech.* (2020) 083203.
- [15] M. Fukuma, D. Kadoh, and N. Matsumoto, Tensor network approach to two-dimensional Yang–Mills theories, *Prog. Theor. Exp. Phys.* **2021**, 123B03 (2021).
- [16] M. Hirasawa, A. Matsumoto, J. Nishimura, and A. Yosprakob, Tensor renormalization group and the volume independence in 2D $U(N)$ and $SU(N)$ gauge theories, *J. High Energy Phys.* **12** (2021) 011.
- [17] P. Milde, J. Bloch, and R. Lohmayer, Tensor-network simulation of the strong-coupling $U(N)$ model, *Proc. Sci., LATTICE2021* (2022) 462 [arXiv:2112.01906].
- [18] T. Kuwahara and A. Tsuchiya, Toward tensor renormalization group study of three-dimensional non-Abelian gauge theory, *Prog. Theor. Exp. Phys.* **2022**, 093B02 (2022).
- [19] S. Akiyama and Y. Kuramashi, Tensor renormalization group study of $(3+1)$ -dimensional Z_2 gauge-Higgs model at finite density, *J. High Energy Phys.* **05** (2022) 102.
- [20] J. Bloch and R. Lohmayer, Grassmann higher-order tensor renormalization group approach for two-dimensional strong-coupling QCD, *Nucl. Phys.* **B986**, 116032 (2023).
- [21] S. Akiyama and Y. Kuramashi, Critical endpoint of $(3+1)$ -dimensional finite density Z_3 gauge-Higgs model with tensor renormalization group, *J. High Energy Phys.* **10** (2023) 077.
- [22] A. Yosprakob, J. Nishimura, and K. Okunishi, A new technique to incorporate multiple fermion flavors in tensor renormalization group method for lattice gauge theories, *J. High Energy Phys.* **11** (2023) 187.
- [23] M. Asaduzzaman, S. Catterall, Y. Meurice, R. Sakai, and G. C. Toga, Tensor network representation of non-Abelian gauge theory coupled to reduced staggered fermions, *J. High Energy Phys.* **05** (2024) 195.
- [24] D. Adachi, T. Okubo, and S. Todo, Anisotropic tensor renormalization group, *Phys. Rev. B* **102**, 054432 (2020).
- [25] H. Oba, Cost reduction of the bond-swapping part in an anisotropic tensor renormalization group, *Prog. Theor. Exp. Phys.* **2020**, 013B02 (2020).
- [26] D. Kadoh and K. Nakayama, Renormalization group on a triad network, arXiv:1912.02414.
- [27] K. Nakayama, Randomized higher-order tensor renormalization group, arXiv:2307.14191.
- [28] Z. Y. Xie, J. Chen, M. P. Qin, J. W. Zhu, L. P. Yang, and T. Xiang, Coarse-graining renormalization by higher-order singular value decomposition, *Phys. Rev. B* **86**, 045139 (2012).
- [29] S. Akiyama, D. Kadoh, Y. Kuramashi, T. Yamashita, and Y. Yoshimura, Tensor renormalization group approach to four-dimensional complex ϕ^4 theory at finite density, *J. High Energy Phys.* **09** (2020) 177.
- [30] S. Akiyama, Y. Kuramashi, T. Yamashita, and Y. Yoshimura, Restoration of chiral symmetry in cold and dense Nambu–Jona-Lasinio model with tensor renormalization group, *J. High Energy Phys.* **01** (2021) 121.
- [31] S. Akiyama, Y. Kuramashi, and Y. Yoshimura, Phase transition of four-dimensional lattice ϕ^4 theory with tensor renormalization group, *Phys. Rev. D* **104**, 034507 (2021).
- [32] J. Bloch, R. G. Jha, R. Lohmayer, and M. Meister, Tensor renormalization group study of the three-dimensional $O(2)$ model, *Phys. Rev. D* **104**, 094517 (2021).
- [33] J. Bloch, R. Lohmayer, S. Schweiss, and J. Unmuth-Yockey, Effective Z_3 model for finite-density QCD with tensor networks, *Proc. Sci. LATTICE2021* (2022) 062 [arXiv:2110.09499].
- [34] R. G. Jha, Tensor renormalization of three-dimensional Potts model, arXiv:2201.01789.
- [35] Y. Liu, Y. Meurice, M. P. Qin, J. Unmuth-Yockey, T. Xiang, Z. Y. Xie, J. F. Yu, and H. Zou, Exact blocking formulas for spin and gauge models, *Phys. Rev. D* **88**, 056005 (2013).
- [36] Y. Meurice, R. Sakai, and J. Unmuth-Yockey, Tensor lattice field theory for renormalization and quantum computing, *Rev. Mod. Phys.* **94**, 025005 (2022).
- [37] A. Yosprakob, Reduced tensor network formulation for non-Abelian gauge theories in arbitrary dimensions, *Prog. Theor. Exp. Phys.* **2024**, 073B05 (2024).
- [38] R. D. Pisarski and F. Wilczek, Remarks on the chiral phase transition in chromodynamics, *Phys. Rev. D* **29**, 338 (1984).

- [39] F. Wilczek, Application of the renormalization group to a second order QCD phase transition, *Int. J. Mod. Phys. A* **07**, 3911 (1992); *Int. J. Mod. Phys. A* **07**, 6951(E) (1992).
- [40] K. Rajagopal and F. Wilczek, Static and dynamic critical phenomena at a second order QCD phase transition, *Nucl. Phys. B* **399**, 395 (1993).
- [41] J. Engels, S. Holtmann, and T. Schulze, The chiral transition of $N(f) = 2$ QCD with fundamental and adjoint fermions, *Proc. Sci. LAT2005* (2006) 148 [arXiv:hep-lat/0509010].
- [42] S. Ejiri, F. Karsch, E. Laermann, C. Miao, S. Mukherjee, P. Petreczky, C. Schmidt, W. Soeldner, and W. Unger, On the magnetic equation of state in $(2 + 1)$ -flavor QCD, *Phys. Rev. D* **80**, 094505 (2009).
- [43] K. Kanaya and S. Kaya, Critical exponents of a three dimensional O(4) spin model, *Phys. Rev. D* **51**, 2404 (1995).
- [44] D. Toussaint, Scaling functions for O(4) in three-dimensions, *Phys. Rev. D* **55**, 362 (1997).
- [45] M. Hasenbusch, Eliminating leading corrections to scaling in the three-dimensional o(n)-symmetric ϕ^4 model: $N = 3$ and 4, *J. Phys. A* **34**, 8221 (2001).
- [46] J. Engels, L. Fromme, and M. Seniuch, Correlation lengths and scaling functions in the three-dimensional O(4) model, *Nucl. Phys. B* **675**, 533 (2003).
- [47] J. Engels and F. Karsch, The scaling functions of the free energy density and its derivatives for the 3d O(4) model, *Phys. Rev. D* **85**, 094506 (2012).
- [48] C. Xu and A. W. W. Ludwig, Nonperturbative effects of topological Θ -term on principal chiral nonlinear sigma models in $(2 + 1)$ dimensions, *Phys. Rev. Lett.* **110**, 200405 (2013).
- [49] X. Luo and Y. Kuramashi, Tensor renormalization group approach to $(1 + 1)$ -dimensional SU(2) principal chiral model at finite density, *Phys. Rev. D* **107**, 094509 (2023).
- [50] J. Zhang, Y. Meurice, and S. W. Tsai, Truncation effects in the charge representation of the O(2) model, *Phys. Rev. B* **103**, 245137 (2021).
- [51] S. Akiyama, R. G. Jha, and J. Unmuth-Yockey, Tensor renormalization group study of 3D principal chiral model, *Proc. Sci. LATTICE2023* (2023) 355 [arXiv:2312.11649].
- [52] A. M. Polyakov, *Gauge Fields and Strings* (Taylor & Francis, London, 1987), Vol. 3.
- [53] J.-M. Drouffe and J.-B. Zuber, Strong coupling and mean field methods in lattice gauge theories, *Phys. Rep.* **102**, 1 (1983).
- [54] M. Campostrini, P. Rossi, and E. Vicari, Strong coupling expansion of chiral models, *Phys. Rev. D* **52**, 358 (1995).
- [55] Z.-C. Gu and X.-G. Wen, Tensor-entanglement-filtering renormalization approach and symmetry-protected topological order, *Phys. Rev. B* **80**, 155131 (2009).
- [56] S. Wang, Z.-Y. Xie, J. Chen, B. Normand, and T. Xiang, Phase transitions of ferromagnetic Potts models on the simple cubic lattice, *Chin. Phys. Lett.* **31**, 070503 (2014).
- [57] J. Chen, H.-J. Liao, H.-D. Xie, X.-J. Han, R.-Z. Huang, S. Cheng, Z.-C. Wei, Z.-Y. Xie, and T. Xiang, Phase transition of the q-state clock model: Duality and tensor renormalization, *Chin. Phys. Lett.* **34**, 050503 (2017).
- [58] S. Akiyama, Y. Kuramashi, T. Yamashita, and Y. Yoshimura, Phase transition of four-dimensional Ising model with higher-order tensor renormalization group, *Phys. Rev. D* **100**, 054510 (2019).
- [59] J. Braun and B. Klein, Scaling functions for the O(4)-model in $d = 3$ dimensions, *Phys. Rev. D* **77**, 096008 (2008).
- [60] <https://qsw.phys.s.u-tokyo.ac.jp/>.